European Journal of Pharmaceutics and Biopharmaceutics 165 (2021) 41–51

Contents lists available at ScienceDirect

European Journal of Pharmaceutics and Biopharmaceutics

journal homepage: www.elsevier.com/locate/ejpb

Etravirine-loaded dissolving microneedle arrays for long-acting delivery

Satish Rojekar [a,b], Lalitkumar K. Vora [a], Ismaiel A. Tekko [a,c], Fabiana Volpe-Zanutto [a], Helen O. McCarthy [a], Pradeep R. Vavia [b,*], Ryan F .Donnelly [a,*]

[a] School of Pharmacy, Queen's University Belfast, 97 Lisburn Road, Belfast BT9 7BL, UK
[b] Department of Pharmaceutical Sciences and Technology, Institute of Chemical Technology, University Under Section 3 of UGC Act – 1956, Elite Status and Center of Excellence – Govt. of Maharashtra, TEQIP Phase III Funded, Mumbai 400019, India
[c] Department of Pharmaceutics and Pharmaceutical Technology, Faculty of Pharmacy, Aleppo University, Syria

ARTICLE INFO

Keywords:
HIV
Microarray patch
Etravirine
Antiretroviral
Microneedle

ABSTRACT

A key challenge of HIV treatment with multiple antiretroviral drugs is patient adherence. Thus, there is an urgent need for long-acting depot systems for delivering drugs over an extended duration. Although the parenteral route is preferred for depot systems, it is associated with obvious drawbacks, such as painful injections, potentially-contaminated sharps waste, and the necessity of trained healthcare personnel for administration. Amongst a small number of alternatives in development microneedles are versatile delivery systems enabling systemic drug delivery and potentially improving patient adherence due to their capacity for self-administration. We have developed dissolving microneedle (DMNs) embedded with etravirine nanosuspension (ETR NS) as a long-acting HIV therapy to improve patient adherence. The ETR NS prepared by sonoprecipitation yielded particle sizes of 764 ± 96.2 nm, polydispersity indices of of 0.23 ± 0.02, and zeta potentials of −19.75 ± 0.55 mV. The DMNs loaded with ETR NS demonstrated 12.84 ± 1.33% ETR deposition in *ex-vivo* neonatal porcine skin after 6 h application. In *in vivo* rat pharmacokinetic studies, the Cmax exhibited by DMNs loaded with ETR powder and ETR NS were 158 ± 10 ng/mL and 177 ± 30 ng/mL, respectively. DMN groups revealed a higher $t_{1/2}$, Tmax, and mean residence time compared to intravenous ETR solutions, suggesting the long-acting potential of etravirine delivered intradermally using DMNs.

1. Introduction

Globally, over 40 million people are infected with human ımmunodeficiency virus (HIV). Committed adherence to Highly Active Antiretroviral Therapy (HAART) is necessary to manage HIV infection [1]. The repeated dosing of numerous drugs in moderately high doses affects patient adherence and reduce the effectiveness of therapy [2,3]. However, HAART cannot provide a long term cure, because it has certain limitations, including the inability to enter into viral reservoirs, adverse reactions, drug resistance and poor pharmacokinetics of anti-retroviral (ARVs) drugs, many of which have very poor water solubility [4].

The development of long-acting drug delivery for ARVs drugs could address many issues, including poor adherence, toxicity and poor pharmacokinetics [5–7]. Etravirine (ETR) is the first second-generation non-nucleoside reverse transcriptase inhibitors (NNRTIs) marketed to treat NNRTI-resistant HIV-1 infection and has been approved for treatment since 2008 [8]. In addition, it is active against the first generation NNRTI-resistant HIV-1. ETR is used with other HIV medications to help control HIV infection [9,10]. This redices the likelihood of other complications, such as new concurrent infections, thus improving quality of life. ETR is generally prescribed to a patient who shows evidence of active viral replication and harbors multidrug-resistant HIV-1 strains and who is already on other HIV medications, such as nevirapine, delavirdine, efavirenz that did not work well enough to control their HIV [8]. ETR has numerous disadvantages over the other anti-HIV drugs specifically related to drug delivery, despite its use in the clinical

Abbreviations: HIV, Human ımmunodeficiency; AIDS, Acquired ımmune deficiency syndrome; ARV, Anti-retroviral; NNRTI, Non-nucleoside reverse transcriptase ınhibitor; MAP, Microarray patch; ETR LA NS, Etravirine long-acting nanosuspension; PVP, Poly(vinylpyrrolidone); PVA, Polyvinyl alcohol; DMNs, Dissolving microneedle; ETR, Etravirine.

* Corresponding authors at: Center for Novel Drug Delivery Systems, Department of Pharmaceutical Sciences and Technology, Institute of Chemical Technology, N. P. Marg, Matunga (E), Mumbai 400 019, India (P.R. Vavia). Chair in Pharmaceutical Technology, School of Pharmacy, Queen's University Belfast, Medical Biology Centre, 97 Lisburn Road, Belfast BT9 7BL, UK (R.F. Donnelly).

E-mail addresses: pr.vavia@ictmumbai.edu.in (P.R. Vavia), r.donnelly@qub.ac.uk (R.F. .Donnelly).

https://doi.org/10.1016/j.ejpb.2021.04.024
Received 15 October 2020; Received in revised form 12 April 2021; Accepted 18 April 2021
Available online 8 May 2021

management of HIV infected patients. Limited pharmacokinetic information is available on its absorption, distribution, and metabolism and excretion following oral administration [11]. ETR has low water solubility and low gastrointestinal permeability and belongs to Class IV of the Biopharmaceutics Classification System. The specific disadvantages of ETR are very low absolute oral bioavailability for commercial Intelence® tablets (0.13%), frequent dosing (200 mg twice a day) and possibly-associated low patient adherence [9,11].

Conventional transdermal delivery is limited by the barrier properties of the outermost skin layer, the *stratum corneum*. A variety of chemical, biochemical, and physical methods have been investigated to improve skin permeability. However, these methods would not be useful for delivering hydrophobic, high-dose anti-HIV drugs across the skin [12,13]. In the case of implantable drug delivery, numerous disadvantages are observed, such as invasiveness, the danger of device failure, termination of devices at the end of therapy, limited use only for highly potent drugs, biocompatibility issues, the possibility of adverse reactions and commercial feasibility [14]. In contrast, microneedles could be fabricated as a low-cost patch that is simple to apply for HIV patients [12,15].

Microneedles (MN) are minimally-invasive, painless, micron size projections (10–900 μm) that penetrate the skin's *stratum corneum* barrier, deposting their cargo in the viable skin layers [16–19]. There are various MN types, including solid MN, drug-coated MN, hydrogel-forming MN and dissolving MN [20–24]. Dissolving microneedles (DMNs) are polymeric, microscopic needles that encapsulate drugs within their matrix. After insertion of DMN into the skin, degradation/dissolution of polymer often starts immediately, releasing the drug for local or systemic delivery over short or long term durations, depending on the nature of the drug and the formulation [15,25]. DMNs are typically prepared from biocompatible polymers and do not generate any hazardous sharps waste since, by definition, they are self-disabling. DMNs are distinct from MN with biodegradable tips prepared from, for example, poly(lactide-co-glycolide) (PLGA), poly(glycolic acid), chitosan or poly(lactic acid). The tips of such needles can dissolve in skin over weeks or even months, but their loading capacity is limited. In contrast, DMNs can potentially load higher doses of drug, but must rely on low drug solubility or drug encapsulation in a controlled release polymer formulation to achieve sustained drug release in the viable skin layers post-MN dissolution, which can often occur within minutes [15,26,27]. The low aqueous solubility of ETR makes it a potenital candidate for sustained dissolution in skin following deposition by DMN [15,28,29–35]. Accordingly, that is what we have focused on, for the first time, in the present work. Both nanosuspension and unprocessed ETR powders were incorprated into DMNs, with the use of various formulation components to enhance performance, and the composite systems extensively evaluated *in vitro* and an *in vivo* rat model.

2. Materials and methods

2.1. Materials

Poly(vinylpyrrolidone) (PVP K29-32) was kindly provided by Ashland (Kidderminster, UK). Poly(vinyl alcohol) (PVA) of molecular weight 9–10 kDa and 31–50 kD, Parafilm® M (~127 μm thickness), HPLC-grade methanol, acetonitrile and acetone were obtained from Sigma-Aldrich (Billingham, Dorset, UK). Etravirine was obtained as a gift sample from Hetero Pharma (Hyderabad, India). All other chemicals were of analytical reagent grade.

2.2. Development of ETR NS

ETR NS was prepared by a solvent evaporation-antisolvent precipitation method. Briefly, 20 mg ETR was dissolved in 1 mL acetone. The organic phase was slowly added by syringe into double-distilled cooled water (<5 °C) consisting of 2% w/v PVA (10 kDa) and 1% w/v PVP (58 kDa) (1:1) maintaining cold conditions [16,43]. PVA and PVP were chosen due to their demonstrated utility in stabilsing nanosuspension formulatuions and their long history of safe use in pharmaceutical products, including injectable preparations. The resulting mixture was subjected to probe sonication for 10-sec pulse on and 5-sec off at the amplitude of 80% (of 125 W, 20 kHz) using a probe sonicator (QS4 system, NanoLab, Waltham, MA, USA) to produce a stable nanosuspension. The organic solvent was evaporated through magnetic stirring (200–400 rpm) overnight at room temperature to yield a colloidally-stable NS. The particle size, polydispersity index (PDI) and zeta potential were analyzed using a particle size analyzer (NanoBrook Omni, Brookhaven, New York, NJ, USA). ETR NS was then subsequently lyophilized and subjected to solid-state characterization.

The effects of solvent, polymer, drug concentration, solvent/anti-solvent ratio and probe sonication time were evaluated in terms of particle size, PDI and zeta potential. In the case of solvent selection, the solubility of ETR was evaluated in acetone, methanol and dichloromethane (DCM). In terms of polymer concentration, 2% w/v PVA (10 kDa) and 1% w/v PVP (58 kDa) were used, respectively [25]. To rationalize drug concentration, ETR NS batches containing various drug concentrations (10, 20, 30, and 50 mg/mL) were prepared [44]. Defined solvent:anti-solvent ratios (0.5:6, 1:6, 1.5:6 v/v in mL) were studied. Probe sonication was carried out for 2, 5, 8 and 10 min, respectively, for the NS preparation and rationalization.

2.2.1. Development of a freeze-drying process for ETR NS

The developed ETR NS (6 mL) contained 50 mg of drug and 2% w/v of PVA (10 kDa) and 1% w/v PVP (58 kDa) as stabilizers. ETR NS was added to freeze-drying vials. ETR NS contains PVP, which acts as a stabilizer and cryoprotectant [45]. ETR NS was pre-frozen in a deep freezer at −75 °C for 12 h and then lyophilized using a VirTis AdVantage 2, Benchtop Freeze Dryer (LabX, Midland, ON, Canada) according to a pre-set regime: Primary drying for 90 min at a shelf temperature of −40 °C, drying for 90 min at a shelf temperature of −30 °C, drying for 90 min at a shelf temperature of −20 °C, drying for 530 min at a shelf temperature of −10 °C and, finally, drying for 90 min at a shelf temperature of 0–10 °C. Secondary drying was carried out for 660 min at a shelf temperature of 25 °C and a vacuum pressure of 50 mTorr [46].

2.3. ETR NS characterization

2.3.1. Particle size analysis and surface charge measurement

Liquid ETR NS and lyophilized ETR NS were analyzed for mean particle size, PDI and zeta potential using the NanoBrook Omni. Briefly, 100 μL of each ETR NS was separately dispersed in 10 mL of Milli-Q water. The measurement was performed at a scattering angle of 90° and temperature of 25 °C. All samples were analyzed in triplicate and mean particle size, PDI and zeta potential were determined.

2.3.2. Drug content analysis of ETR NS

Aliquots of 10 mg from each of three batches of freeze-dried ETR NS were separately dissolved in 1 mL of acetonitrile. The samples were sonicated for 30 min and then centrifuged at 10,000 rpm for 15 min. ETR contents were analysed, after suitable dilution, by the validated reversed-phase high-performance liquid chromatography (RP-HPLC) method described in the pharmaceutical analysis Section 2.4.3.

2.3.3. DSC, FTIR and SEM analysis

ETR, freeze-dried ETR NS and physical mixtures of ETR and other constituents were analyzed by differential scanning calorimetry (DSC) (DSC Q100, TA instruments, Newcastle, DE, USA) at a heating rate of 10 °C/min from 30 °C to 300 to study the phase transition. A Shimadzu IRAffinity-1S infrared spectrophotometer (Shimadzu, Buckinghamshire, UK) was used to analyze ETR, freeze-dried ETR NS, and physical mixtures of ETR and other constituents. ETR NS and ETR loaded DMNs were mounted onto an aluminium stub and observed under a TM3030

microscope (Hitachi Ltd, Tokyo, Japan).

2.3.4. In vitro drug release from freeze-dried ETR NS

In vitro release studies were carried out for the ETR NS and plain ETR powder using a dialysis bag technique [16]. An ETR content equivalent to 10 mg ETR of ETR and ETR NS was separately sealed in the cellulosic dialysis membrane of cut-off 12–14 kDa (Spectrum Laboratories Inc., Piscataway, NJ, USA). Then it was placed into a beaker containing 150 mL of phosphate buffered saline (PBS, pH 7.4) and 1% w/v Tween 80 and loaded into a shaker-incubator (Incu S-series, Incu-50S, SciQuip, Shropshire, UK) operating at 100 rpm and maintained at 37 ± 0.5 °C. At pre-defined time intervals, 1 mL of the release medium was removed and replaced by an equivalent volume of fresh pre-warmed release medium. The samples were evaluated for ETR content by the validated RP-HPLC method. Commonly-used drug release kinetic models were applied to understand the mechanism of drug release from the ETR NS. Specifically, the drug release data was analyzed according to zero order, first order, Higuchi square root and Korsmeyer- Peppas models. The most appropriate model(s) were chosen based on the goodness of fit test [47].

2.4. Pharmaceutical analysis

2.4.1. Instrumentation and chromatographic conditions

RP-HPLC was carried out to quantify ETR using an Agilent 1200® binary Pump, standard autosampler, variable wavelength detector (Agilent Technologies UK Ltd., Stockport, UK) and detection was at 308 nm. Chromatographic separation was performed using a Symmetry® (3.9 mm x150 RP-18) column with 5 μm packing and isocratic elution with a flow rate 1 mL/min. The mobile phase was a combination of acetonitrile:methanol: phosphate buffer, pH 6.5 (40: 25: 35 v/v). The ETR standard solutions were made by diluting suitable volumes of acetonitrile stock solution (100 μg/mL) to give final concentrations of 2, 4, 6, 8, 10, 12, 14 and 16 μg/mL. Afterwards, 20 μL of each solution was injected onto the RP-HPLC [48,49]. The method was validated for accuracy and recovery (˃90%), linearity (2–14 μg/mL, r2 = 0.999, y = 139.45x + 6.0705), specificity, precision (% CV 1.71), limit of quantitation (LOQ, 0.997 μg/ml) and limit of detection (LOD, 0.329 μg/ml) as per the ICH (International Council on Harmonization of technical requirements for pharmaceuticals for human use) guidelines [50]. The representative HPLC graph is shown in Supplementary Data (Fig. S2).

2.4.2. ETR extraction efficiency from the skin

Full-thickness excised neonatal procine skin (obtained from stillborn piglets and immediately frozen at −20 °C and defrosted overnight prior to use) was carefully shaved using disposable razors (Gillette Blue II™, Gillette, Reading, UK) and subsequently equilibrated with phosphate buffered saline. The ETR solution was incubated with the excised skin at 37° ± 0.5 °C for 24 h. The skin sample was then cut into small pieces using scissors and was homogenised using a TissueLyser LT™ (QIAGEN, Manchester, UK). Each sample was vortexed for 20 min with 500 μL water and stainless steel beads (5 mm, QIAGEN, Manchester, UK). Next, 1 mL of acetonitrile was added and samples were sonicated for 30 min for drug extraction and centrifuged at 14,800 rpm for 10 min. The supernatant of approximately 100 μL was taken and diluted with 900 μL of acetonitrile and subsequently analyzed by RP-HPLC.

2.4.3. LC-MS analysis

ETR quantification from rat plasma was performed using liquid chromatography-mass spectrometry (LC-MS). The chromatographic separation of ETR was performed on a Symmetry® (3.9 mm x150 RP-18) column with 5 μm packing. The vaporizer functioned at 350 °C; 40 psi nebulizer gas pressure and 4000 V capillary voltage were set. The ETR was detected by its positive ion (*m/z* 436.0) with single ion monitoring. Mobile phase A comprised of 0.1% formic acid in water and mobile phase B of acetonitrile. Aliquots of 10 μL were injected for the analysis. Moreover, isocratic elution was carried out with the mobile phase ratio % A:B (70:30) and a flow rate of 0.6 mL/min for 8 min. ETR rat plasma content was quantified using the validated LC-MS methodology. The plasma samples were evaluated using Agilent ChemStation® Software B.02.01. The LC-MS method was validated, as per the ICH guidelines for the linearity (10–10000 ng/mL, r^2:0.999, y = 96.735x + 2252.6), accuracy and recovery (˃90%), precision and specificity (repeatability % CV 0.09), LOQ (7.28 ng/mL) and LOD (2.40 ng/mL) [51].The representative LC-MS spectra of 50 ng/mL of ETR spiked in blood plasma is shown in Supplementary Data Fig. S3).

2.5. ETR loaded DMNs fabrication

DMNs arrays were prepared for the ETR NS and plain ETR powder. The DMNs were formulated from the same polymers that were used in the ETR NS preparation. The first layer of MN was prepared from freeze-dried ETR NS to produce DMNs with 50% w/w ETR content. Aliquots of 500 mg of freeze-dried ETR NS were mixed with 700 mg of distilled water and subsequently *cyclo*-mixed at 2000 rpm for 10 min. Approximately 500 mg ETR NS-loaded gel was transferred into poly(dimethylsiloxane) mould templates (16 × 16) then placed in a positive air pressure chamber for 3 min at 5 bar [52]. After the silicone moulds were removed from the pressure chamber, excess ETR NS loaded mixture was removed from the surface by spatula and the mould was placed in the positive pressure chamber for 30 min at 5 bar. The pressure was released gradually over 5 min and the silicone moulds were then dried under ambient conditions for 24 h. The second layer of DMNs was prepared from an aqueous mixture of 40% w/w PVP K29-32 (M.W: 58 kDa) aqueous gel and 30% w/w PVA (M.W: 31–50 kDa) aqueous gel (50:50 mix). This final gel was mixed first with a spatula for 10 min and then centrifuged for 15 min at 3500 rpm. The gel was left to settle overnight before use. After that, this gel mixture was cast over the first layer under vacuum and then transferred into the positive pressure chamber for 15 min at 5 bar. The pressure was released gradually over 5 min and the silicone moulds were dried for 24 h at 37 °C. DMN arrays were removed from the moulds and visually evaluated for successful needle formation. A similar method was adopted to prepare the ETR powder loaded DMNs [16,28].

2.6. Characterization of dissolving microneedle arrays

2.6.1. Drug content determination

The ETR NS loaded DMNs were analysed for drug content by dissolving each DMNs in 1 mL water. Then, 10 μL was collected into 1.5 mL tubes and mixed with 190 μL distilled water and 0.8 mL acetonitrile to allowed polymer precipitation, whereas the drug remained dissolved. Subsequently, 100 μL of this solution was mixed with 0.9 mL acetonitrile and centrifuged (Eppendorf Minispin® centrifuge, Eppendorf, Stevenage, UK) at 14,800 rpm for 15 min. The supernatant was collected and analysed by RP-HPLC.

2.6.2. Effect of DMNs casting on the ETR NS particle size

DMNs were dissolved in water by using a magnetic stirrer at 200–400 rpm. The mean particle sizes and PDI of these dispersions were analyzed in triplicate using the particle sizer [53].

2.6.3. Mechanical and insertion properties of ETR NS loaded DMNs

2.6.3.1. Compression studies. The mechanical properties of the DMNs were evaluated using a TA.XT-Plus Texture Analyser in compression mode (Stable Microsystem, Haslemere, UK) [54]. The initial height of DMNs was measured using Leica EZ4D digital microscope (Leica, Milton Keynes, UK). Afterwards, DMNs were attached by double-sided adhesive tape to the movable cylindrical probe of the Texture Analyzer. DMNs were compressed against the flat aluminium base of the Texture Analyser at a force of 32 N (8 N/needle) and a speed of 0.5 mm/sec for 30

sec. Pre-test and post-test speeds were fixed at 1 mm/sec and a 0.049 N trigger force was set. DMN heights were determined using the Leica EZ4D digital microscope. The % reduction of height after applying the axial compression load was determined [55]. The % change in height was calculated using Equation (1) [38].

$$\%\textbf{\textit{Height reduction}} = \frac{\textbf{\textit{original height}} - \textbf{\textit{new height}}}{\textbf{\textit{original height}}} \times 100 \quad (1)$$

2.6.3.2. Insertion properties into Parafilm M®. The DMNs was evaluated for their insertion properties into Parafilm M® (Bemis Company Inc., Soignies, Belgium). This flexible thermoplastic sheet prepared from olefin-type material was used for the study [56]. Parafilm M® was previsouly validated as a skin simulant for microneedle penetration studies [25,56]. The initial height of DMNs was measured using the Leica EZ4D digital microscope. Later, the Parafilm M® sheet was gently folded into an eight-layer film (≈1 mm thickness). Subsequently, DMNs were attached to the movable probe of the Texture Analyzer. Then, the probe was lowered onto the folded Parafilm M® at a speed of 1.19 mm/sec, using a defined force of 32 N applied for 30 sec [25,55,56]. Then, the Parafilm M® sheet was carefully unfolded and, subsequently, the number of holes generated in each layer was measured using the Leica EZ4D digital microscope [55].

2.6.3.3. Insertion properties into full-thickness neonatal porcine skin. In order to establish the insertion depth of the ETR loaded DMNs into excised full-thickness neonatal porcine skin, optical coherence tomography (OCT) was employed as previously reported [57]. The inserted DMNs (32 N, 30 sec using the Texcture Analyser) were immediately observed by the EX1301 OCT Microscope (Michelson Diagnostics Ltd., Kent, UK). The OCT system has a laser center wavelength of 1305 ± 15 nm. This enables real-time high-resolution imaging (7.5 mm lateral and 10.0 mm vertical resolution). Moreover, the skin was studied at a frame rate of the 15B-scans (2D cross-sectional scans) per second with a scan width of 5.0 mm. The 2D images were evaluated by ImageJ® (National Institutes of Health, Bethesda, MD, USA). The image scale was 1.0 pixel = 4.2 mm, allowing the depth of DMNs penetration to be determined [38].

2.6.3.4. Ex vivo drug deposition of ETR loaded DMNs. The skin deposition of the ETR loaded DMNs was studied again using full-thickness excised neonatal porcine skin [58]. The skin sample was tagain carefully shaved (barrier function maintannce confirmed by transepidermal water loss measurments with a Deflin Vapometer™, Delfin technologies Ltd., Kuopio, Finland) and subsequently equilibrated with phosphate buffered saline before mounting onto a weighting boat lined with phosphate buffered saline-saturated absorbent paper. The ETR loaded DMNs were inserted in the skin with thumb pressure over 30 secs, and a 20 g stainless steel cylindrical weight was kept on the skin for DMNs fixation. The skin was incubated for 6 h at 37 °C. DMNs were removed at a specified time points of 1 h and 6 h and images were taken using the digital microscope [28]. Skin samples were then sliced into small parts by scissors. Skin was then homogenized using the TissueLyser LT™ and drug extracted and quantified as described above (Section 2.4.2).

2.7. Stability studies

DMNs arrays incorporating ETR were stored under sealed packaging conditions. The glass vials containing DMNs were capped and further sealed with Parafilm® and then stored at room temperature in evacuated chambers. The DMNs were then dissolved and assayed for drug content, particle size, PDI and mechanical properties at 0, 1, 2, 3, and 4 weeks, as described above. RP-HPLC determined the percentage recovery of ETR.

2.8. In vivo studies

The Ethical Committee of the Queen's University Belfast Biological Services Unit (BSU) reviwed study design and provided permission for the *in vivo* study of the ETR and ETR NS loaded DMNs. This study was carried out under Project Licence No. 2794 and Personal Licences 1747 and 1892.

The experiment was conducted using female Sprague Dawley rats (195 ± 8 gm) aged between 8 and 12 weeks. Animals were adapted for 7 days before starting the study. The animals had fasted overnight before parenteral and intradermal dosing. The animals were divided into three groups: Group 1- each rat received a control IV injection of ETR solution 2.5 mg/kg; Group 2- each rat received 4 ETR NS loaded DMNs; Group 3- each rat received 4 ETR powder loaded DMNs. The rats were anaesthetized using gas anaesthesia (2–4% isoflurane in oxygen). Animal hair was then removed using electrical clippers and Boots Expert® depilatory cream (The Boots Company PLC, Nottingham, UK) 24 h before drug delivery, with skin barrier integrity again confirmed using the Vapometer™. The rats were again anaesthetized immediately before the application of the DMNs. Group 1 (n = 6) was given intravenous administration by tail vein; ETR solution of 2.5 mg/kg (3.5 mg/mL dissolved in dimethyl sulfoxide). Four DMNs arrays (1.2 mg/ DMNs patch) were fixed on the approximate 1.6 cm^2 area and held in place by adhesive foam (TG Eakin Ltd, Comber, Co. Down, UK) for the Group 2 (n = 5) ETR NS loaded DMNs and Group 3 (n = 4) ETR powder loaded DMNs, respectively. DMNs were applied opposite each other by firm finger pressure on a strained section of the skin on each rat's back. After the application of DMNs, a vapor-permeable dressing (Tegaderm™, 3 M, Bracknell, UK) was carefully applied over all DMNs arrays. The DMNs were further secured by gently wrapping the animals using Kinesiology tape (KT Health, American Fork, UT, USA) to prevent animals from removing the DMNs. Then animals were shifted into single cages. Blood samples (200 μL per sample) were collected in heparinized microcentrifuge tubes from tail veins using cannulated syringes. Plasma separation was carried out by centrifuging the blood at 5200 rpm for 15 min at 4 °C.

Separated plasma samples were then stored at −20 °C until analyzed. All samples were uniformly processed for drug extraction from the plasma using liquid-liquid extraction methods. In detail, 100 μL of plasma was taken and then 300 μL of acetonitrile was added and samples vortexed for 15 min. All sample were then centrifuged at 14,800 rpm for 15 min at 4 °C. The supernatant were then analyzed by LC-MS method. The non-compartmental extravascular pharmacokinetics were evaluated using standard techniques by the PKSolver add-in program in Microsoft Excel (Microsoft Corporation, Redmond, WA, USA). The drug's maximum plasma concentration (Cmax) was assessed from the plasma drug concentration versus time profile. The dose normalization is a simple calculation performed using the pharmacokinetic parameters. Here, we have divided the PK parameters by the different administered doses. We have performed it for individual treated and untreated groups. This method should only be performed on exposure parameters (Cmax, AUC, Cmin, etc.) [59]. All the major *in vivo* pharmacokinetics were summarized and statistical comparisons were performed after normalization [28,35].

2.9. Statistical analysis

The data were represented as means ± standard deviation (SD) of the mean. The statistical assessment among particle size and PDI during ETR nanosuspension development was made using an Unpaired *t*-test by Graphpad Prism software (ver. 6; Graphpad, Inc., San Diego, USA). The $p < 0.05$ value denoted statistical significance.

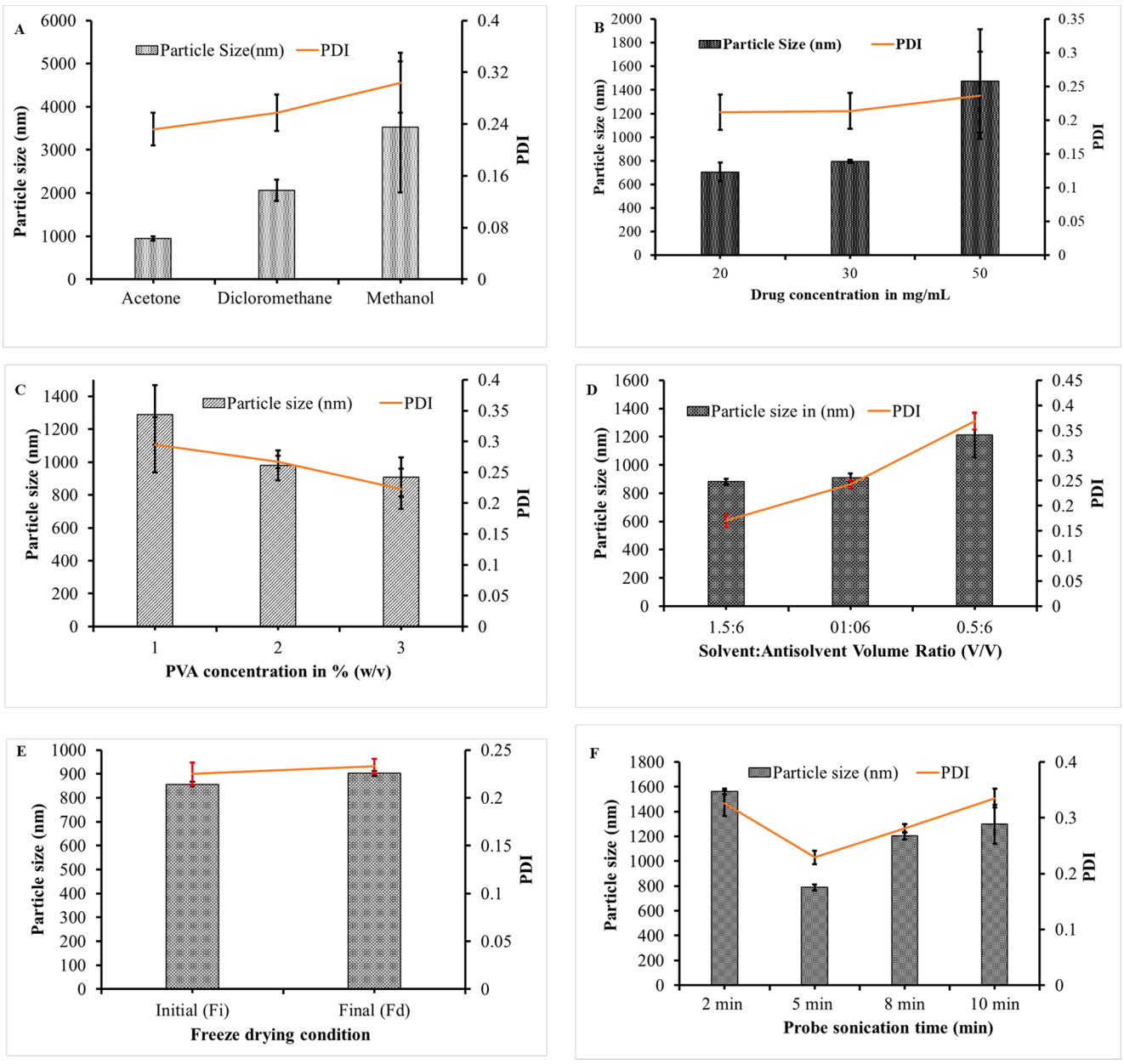

Fig. 1. (A) Effect of different organic solvents, (B) drug concentration, (C) different concentrations of PVA (D) solvent: antisolvent ratio, (E) probe sonication time, and (F) freeze-drying on the particle size and PDI (means ± SD, n = 3).

3. Result and discussion

3.1. ETR nanosuspensions development

ETR NS was developed by a bottom-up approach using the sono-precipitation technique, which involves the addition of an organic solution containing drug solubilized in an anti-solvent along with a stabilizer. This leads to the rapid precipitation of drugs because of desolvation, producing nano-sized drug particles. This method abides by the Ostwald–Mier theory, according to which crystallization commences while reaching the supersaturation stage, followed by nucleation and crystal growth [39,60]. However, after the addition of saturated organic drug solution to the anti-solvent, supersaturation occurs, with desolvation resulting in the generation of a larger number of nuclei and sustained crystal growth. The nanoprecipitation involves various critical parameters such as drug concentration, probe sonication, selection of solvent, antisolvent and stabilizer [61–64].

3.1.1. Effect of solvent

With a combination of 2% w/v PVA (10 kDa) and 1% w/v PVP (36 kDa) and a drug concentration of 30 mg/mL, it was observed that the lowest particle size of 951 ± 106 nm was obtained using acetone followed by dichloromethane and then methanol, respectively, as shown in Fig. 1 A. PDI results showedthe lowest PDI was obtained using acetone, followed by DCM and then methanol, respectively (Fig. 1A). Significant differences between formulations prepared with acetone and DCM in terms of particle size and PDI were observed. Thus, it was decided to use acetone as a solvent in this study [16,39,61].

3.1.2. Effect of drug concentration

Increasing the amount of drug from 20 mg/mL to 50 mg/mL resulted in a significant difference ($p = 0.019$) in terms of particle size, but not PDI values (Fig. 1B).

3.1.3. Effect of stabilizer

The stabilizer's key role is aiding in particles' wetting, thereby preventing Ostwald ripening and aggregation of nanoparticles to obtain a physically stable formulation [65,66]. The mean particle size and PDI decreased as PVA concentration was increased keeping the concentration of PVP (36 kDa) at 1% w/v and drug at 30 mg/mL, respectively (Fig. 1C).

3.1.4. Effect of solvent: anti-solvent ratio

The effect of the solvent/antisolvent ratio on particle size and PDI was evluated for a set drug concentration of 30 mg/mL. The concentrations of stabilizers were fixed at 2% w/v PVA (10 kDa) and 1% w/v PVP (58 kDa), respectively. Probe sonication was performed for 5 min at a solvent/antisolvent ratio of 1.5/6 v/v in mL and it was found to be the most favorable. Larger particles were obtained when the solvent concentration ratio was reduced while keeping the sonication time constant at 5 min (Fig. 1E).

3.1.5. Effect of probe sonication time

The effect of probe sonication time on particle size and PDI were evaluated at different probe sonication times of 2, 5, 8 and 10 min with a constant drug concentration (30 mg/mL), 2% w/v PVA (10 kDa) and 1% w/v PVP (58 kDa) (Fig. 1E). Particle size initially decreased with an increase in the probe sonication to 5 min. A significant difference in particle size ($p = 0.001$) was observed in each case between 5 min and longer probe sonication times. This phenomenon was probably observed due to a rise in the nucleation rate induced by ultrasonication [44,61,67–70].

3.1.6. Development of the freeze-drying process

The freeze-drying process was used to obtained free-flowing powder for process feasibility and solid-state characterization of developed ETR NS. The developed freeze-dried ETR NS was obtained with 30 mg/mL drug and 2% w/v PVA (10 kDa), with 1% w/w of PVP 58 kDa, acting as both co-stabilizer and cryoprotectant [68]. The solvent to antisolvent ratio (1.5:6 v/v) and 80% of sonication amplitude for 5 min were finalized at this stage as the production parameters. The particle size and PDI of the developed NS were initially (fi, prior to lyophilization) found to be 856 ± 126 nm and 0.24 ± 0.03, and finally (fd, after the lyophilization) 902 ± 149 and 0.23 ± 0.01, respectively. The fi/fd ratio was found to be 0.94. After the evaporation of the solvent, a freshly prepared ETR NS was immediately lyophilized to maximise drug-loading in DMNs

3.2. ETR NS characterization

3.2.1. Drug content analysis

RP-HPLC assayed ETR NS for determining the % drug content; it was found to be 99 ± 3.2%. The yield values for lyophilized nanosuspensions were between 94 and 98%.

3.2.2. DSC, FTIR and SEM analysis of ETR NS

SEM (Scanning electron microscopy) was used for surface topography of the developed ETR NS and plain ETR powder to understand morphological changes after converting crystalline ETR to amorphous ETR. The ETR NS were aggregated in nature, and the plain ETR was crystalline rod shaped. From SEM images, plain ETR powder particle size was found to be more than 30 μm, and ETR NS particle size was, obviously, less than 1 μm (data was not shown) [65]. The meting point of ETR NS was lower than the ETR powder and physical mixture of ETR and stabilizers, because of the impact of the particle size reduction and subsequently enhanced surface area of nanoparticles and amorphization of ETR (Supplementary data, Fig. S1 A). [71,72]. The FTIR analysis was performed for ETR, ETR NS and ETR PVA PVP physical mixture to understand the interaction between ETR and PVA and PVP as a stabilizer. Moreover, no chemical interactions were observed in the case of the ETR NS and ETR PVA PVP physical mixture. FTIR spectra retained all the characteristic peaks of ETR (Supplementary data, Fig. S1 B). [72,73].

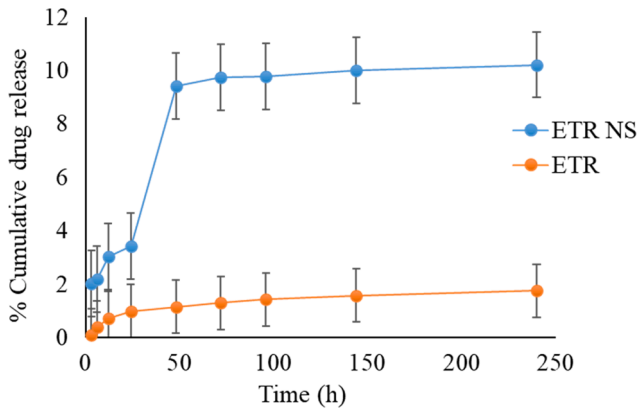

Fig. 2. *In vitro* drug release study of ETR and the lyophilized ETR NS (means ± SD, $n = 3$).

3.2.3. In vitro drug release from freeze-dried ETR NS

The plain ETR powder, 10 mg, was dispersed in 2 mL of pH 7.4 phosphate buffered saline containing 1% w/v Tween 80. The lyophilized ETR NS showed considerably higher release than that of the ETR powder. After 240 h, 10 ± 1% (1 mg) of the drug was released from the lyophilized ETR NS compared with 1.7 ± 0.04% (0.17 mg) released from the ETR powder (Fig. 2). The enhanced dissolution rate of ETR NS could be ascribed to the noticeable reduction in particle size and the subsequently increased surface area [74–76]. The release profile of the developed ETR NS formulation was fitted to several drug release kinetic models so as to understand the mechanism of release of ETR from ETR NS. The developed formulation's drug release pattern indicated the best fit with the first order model ($r^2 = 0.9997$) [47].

3.3. Characterization of ETR NS loaded DMNs

3.3.1. Drug content from ETR NS loaded DMNs

Drug content was analyzed using RP-HPLC and it was found that each ETR NS-loaded DMN array contained approximately 1206 ± 120 μg. ETR NS was loaded only in the tip parts, as shown in Fig. 4 E & F.

3.3.2. ETR NS particle size analysis

The effect of DMN casting on particle size and PDI of the ETR NS was evaluated. The ETR NS had mean particle size of 793 ± 88.2 nm and mean PDI of 0.28 ± 0.03 PDI after DMN drying, subsequent dissolution and particle analysis. Such parameters were not significantly altered compared to the lyophilized formulation (Section 3.1.6), possibly due to stabilization by the dried polymeric matrix of the DMNs The NS-loaded DMNs had a more homogenous appearance that those prepared using the plain ETR powder.

3.3.3. Mechanical testing of ETR NS loaded DMNs

DMNs must be mechanically-robust so as to withstand handling and skin insertion. Following the 32 N per array axial load application, the ETR NS loaded DMNs exhibited only a 7 ± 1.5% height reduction (Fig. 3 B, C, and D). This force of 32 N per array has been previosuly shown to be the mean force applied by human volunteers while inserting microneedles into their skin [55].

3.3.4. Insertion properties into Parafilm M®

This study was performed using ETR NS loaded DMNs by inserting them into a stack of 8-layer Parafilm M® and then evaluating the insertion depth of the DMNs shafts indirectly by measuring the distance between the DMNs baseplate and the first layer of the Parafilm M® (Fig. 3 A). ETR NS loaded DMNs penetrated to the third layer of Parafilm

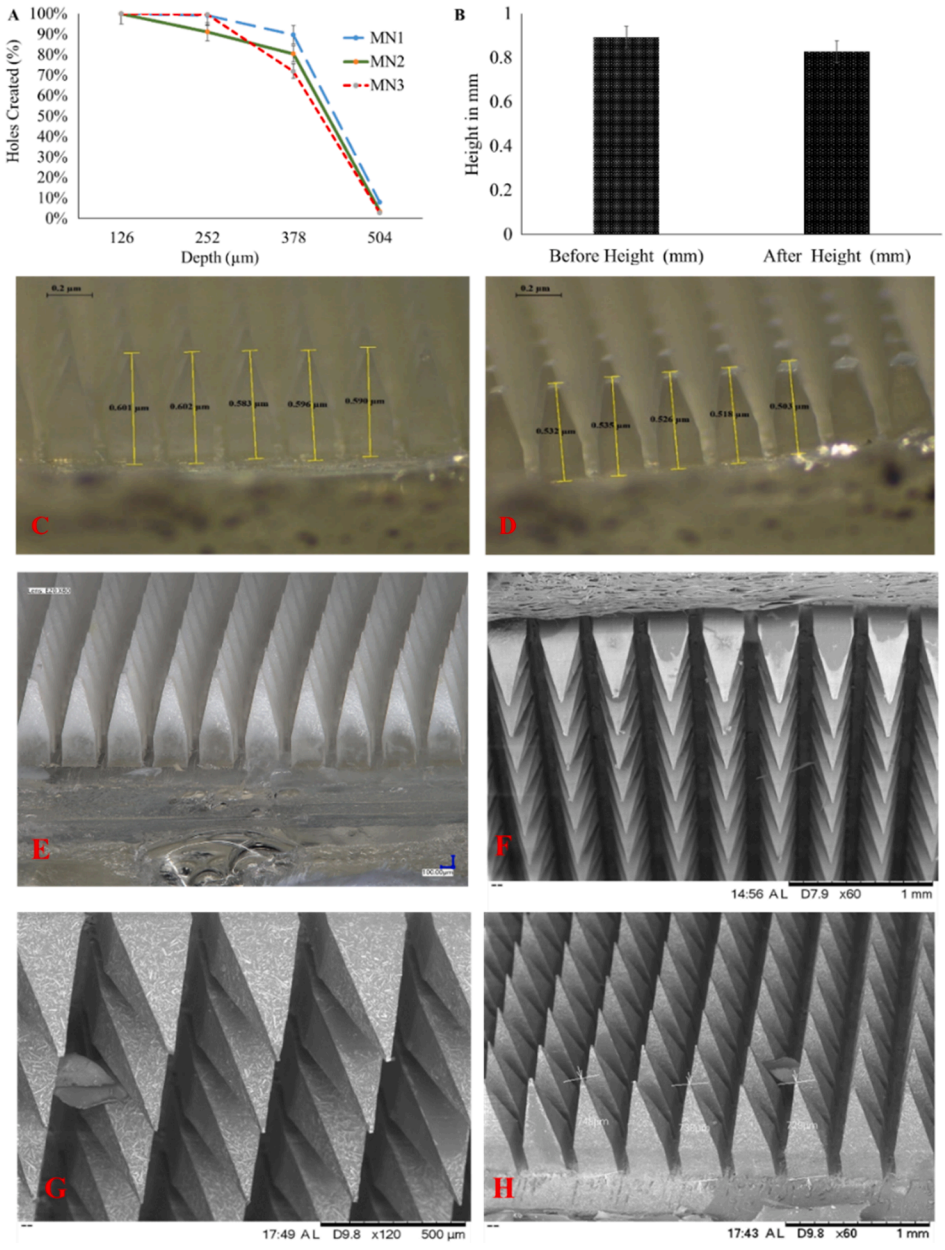

Fig. 3. (A) % of holes generated in each Parafilm M® layer and their related insertion depth, application of a force of 32 N for ETR NS loaded DMNs, (B) % reduction in the height of DMNs upon applied a force of 32 N at 0.5 m/sec, for 30 sec (means ± SD, n = 3), (C) MN height pre-compression, (D) MN height pre-compression(32 N), (E) Microscopic images of ETR loaded DMNs. Representative SEM images of ETR NS loaded MN, showing, (F) Needle tip and containing ETR NS loaded DMNs) and (G) Needle tip containing ETR (H) row of individual needles containing ETR.

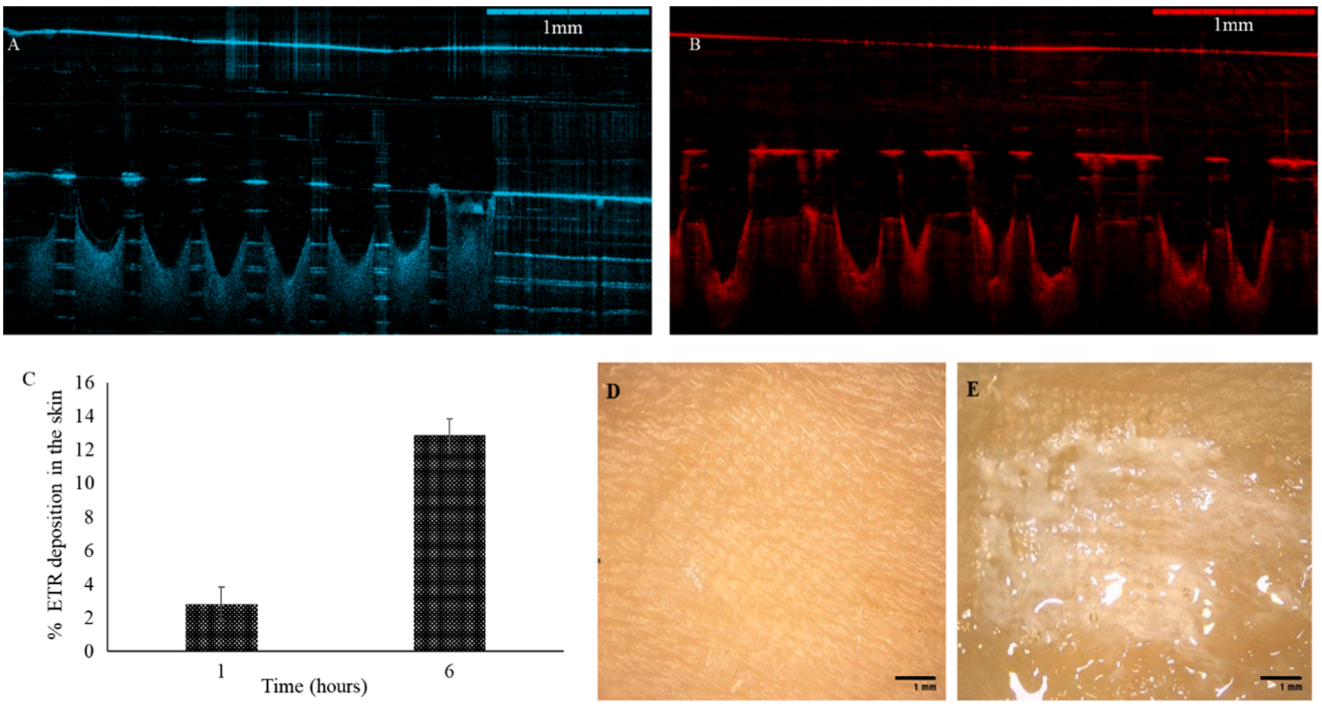

Fig. 4. OCT images after insertion of ETR NS loaded DMNs arrays into; (A) 8-layers of Parafilm M® (B) full-thickness neonatal porcine skin. (C) % Skin drug deposition in excised neonatal porcine skin (means ± S.D., n = 3). Digital image of skin after application of ETR NS loaded DMNs at; D) 1 h and (E) 6 h.

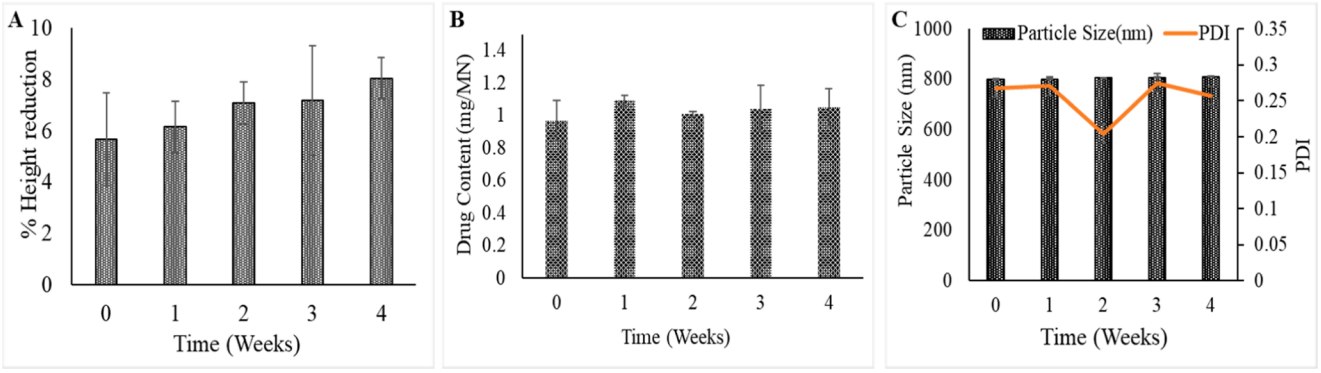

Fig. 5. Four-week stability of dissolving ETR NS loaded DMNs at 25 °C storage conditions sealed containers; (A) Effect on mechanical strength, (B) Drug content and (C) Effect on particle size and PDI, (means ± S.D., n = 3).

M®. Thus, it was determined that the DMN insertion depth was between 378 μm and 504 μm of the total 850 μm of the needle height [56].

3.3.5. *Ex vivo insertion properties*

OCT was employed to obtain real-time images of insertion of the ETR NS loaded DMNs arrays into the Parafilm M® layers and the neonatal porcine skin. The insertion depth in excised neonatal porcine skin was 300–350 μm. However, Parafilm M® was penetrated down to around 378 μm, as indicated in Fig. 3 A. This is similar to the previous insertion studies of the DMNs into Parafilm M® [56].

3.3.6. *Scanning electron microscopy*

The morphology of the developed and optimized ETR and ETR NS containing DMNs were evaluated under SEM, showing pyramidal portions of around 545 ± 5 μm attached to columns measuring 180 ± 3 μm. Fig. 3 F, G and H represent the SEM images of dissolving DMNs, containing tip-loaded ETR NS and, spearately, plain ETR powder.

3.3.7. *Ex vivo skin deposition of ETR NS loaded DMNs*

The ex vivo skin deposition of the ETR NS loaded DMNs was found to be 155 ± 16 μg per ETR NS loaded DMN array, equating to a deposition of 12.84 ± 1.33% of drug payload in excised neonatal porcine skin.

Table 1
Pharmacokinetic parameters after intravenous administration of ETR solution (2.5 mg/kg body weight), ETR NS loaded DMNs, and ETR powder loaded DMNs (total four patches per animal, 1.2 mg/per patches) in the female Sprague Dawley rats.

Parameter	ETR Intravenous 2.5 mg/kg per rat	ETR loaded DMNs Intradermal 1.2 mg/ MN (4 patches/per animal)	ETR NS loaded DMNs Intradermal 1.2 mg/ MN (4 patches/per animal)
T_{max} (h)	1	168	168
C_{max} (ng/mL)	2010 ± 128	158 ± 10	177 ± 30
AUC (μg h/mL)	37.56	96.06	107.06
t/2 (h)	136 ± 4.6	222 ± 16.60	249 ± 21.63
MRT 0-inf_obs (h)	163 ± 76	451 ± 65	480 ± 69
Vss_obs (mg/ng/mL)	0.001	0.014	0.014
CL (mg)/(ng/mL)/h	0.0018	0.000044	0.000039

3.4. Stability testing of ETR NS loaded DMNs

The stability study of the developed and optimized DMNs was performed to assess change in the mechanical properties, drug content and particle size, and PDI during storage. The DMNs arrays incorporating ETR NS were found to be stable for four weeks at a storage temperature of 25 °C (Fig. 5 A, B, and C). DMNs showed unchanged physical appearance after four weeks. The drug content of ETR NS loaded DMNs were in the range between 0.96 ± 0.12 to 1.05 ± 0.11 mg/DMN. No appreciable effect was seen on the particle size, PDI and mechanical strength.

3.5. In vivo studies

It was observed that the DMNs dissolved within 24 h of application, which was interesting to note, as these DMNs have a high content of poorly water-soluble drug particles, having log P of 5 [11]. Most importantly, no sign of irritation on the skin of the rats was observed. Pharmakokinetic parameteres are presented in Table 1

Fig. 6 A and B show the plasma concentrations versus the time curves for rats treated with ETR IV injection, ETR NS-loaded DMNs, and ETR powder-loaded DMNs. The time required to attain Cmax (maximum plasma drug concentration) was ~1 h in the case of the parenteral group, whereas for ETR NS and ETR loaded DMNs groups it was 168 h post-patch application.

In vivo studies showed that, after IV administration, ETR solution was quickly cleared from the circulation. However, plasma levels generated by intradermal deposition of ETR NS and ETR powder remained elevated for prolonged periods, which indicated the extended-release from ETR NS and ETR powder [77]. Cmax (2010 ± 128 ng/mL) was reached within 1 h (T_{max}) after IV dosing of ETR. However, Cmax for the ETR NS- and ETR powder-loaded DMNs were 177 ± 30 ng/mL and 158 ± 10 ng/mL, respectively, at 168 h (T_{max}), as shown in Table 1. This is most likley due to slow dissolution and, thus absoprtion from the intradermal ETR depots [5,78,79].

After dose normalization calculations, the C_{max} for the ETR NS- and ETR powder-loaded DMNs were decreased 21.80 and 24.43-folds, respectively, compared to the IV reference group, as shown in Table 1. This could again be attributed to the slower release of the hydrophobic ETR particles in the skin interstitial fluid, with subsequent slower absorption into the systemic circulation [28,79].

The areas under the curves (AUCs) for ETR NS and ETR loaded DMNs were increased respectively by 1.48 and 1.33-folds compared to the ETR IV injection (Table 1), confirming a much more prolonged plasma exposure [6,7,80].

The mean plasma concentration for the ETR solution administered by IV route was found to be 218 ± 34 ng/mL at 24 h. However, in the case of ETR NS and ETR loaded DMNs were found to be 116 ± 15 ng/mL and 122 ± 23 ng/mL, respectively. This confirms the rapid clearance of the ETR when given intravenously, as compared to intradermal solid drug depots. Indeed, the plasma levels induced by the DMNs continued to increase up to 168 h, which could be attributed to the sustained dissolution/absorption of the ETR from these depots [28,53]. Plasma profiles of ETR delivered intradermally using DMNs did not show marked differences between the ETR NS and ETR powder.

The mean residence time (MRT) refers to the time of residence of a drug in the body prior to elimination. This is, in turn, closely related to kinetic processes, such as dissolution rate of a drug depot, rate and extent of the absorption process, as well as distribution and elimination phenomena. In the present work, the MRTs or ETR delivered using DMNs laoded with ETR NS or ETR powder were found to be 449 h and 430 h, respectively, both significantly higher ($p < 0.03$) than that of the ETR IV solution (Table 1). This indicates that ETR remained in the body for a longer time, which is attributable to the extended-release potential of the ETR NS- and ETR powder-loaded DMNs [81–83].

ETR can be used for the population whose HIV disease is resistant to NNRTIs and other ARV drugs [84]. We have compared the available pharmacokinetic data for the marketed Intelence® tablet (200 mg/kg dosed as a suspension of ground tablets) with our data for ETR NS- and ETR powder-loaded DMNs in female Sprague Dawley rats after dose

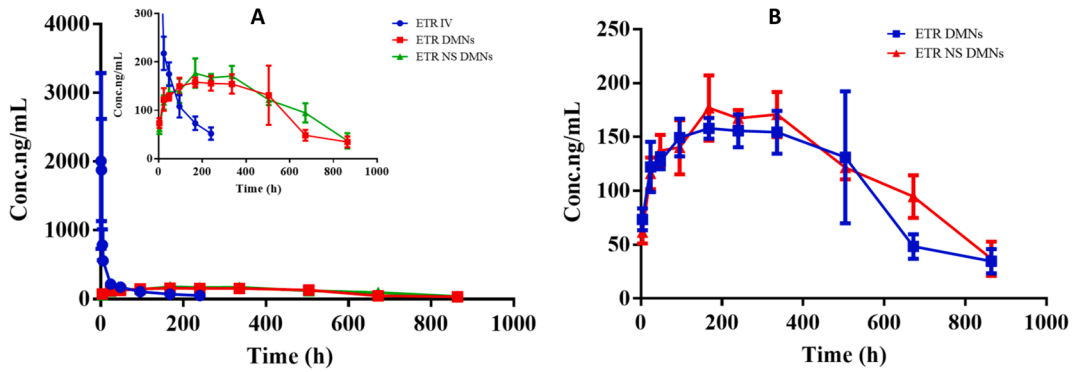

Fig. 6. (A) plasma concentration–time profiles after a single 2.5-mg/kg dose of the ETR solution in female rats (n = 6, alternated sampling per treatment group); ETR NS loaded DMNs and ETR Loaded DMNs (n = 5 & 4), showing the effect of dose and route of administration and (B) 36-days mean plasma concentration-time profiles of ETR after intradermal application of 4.8 mg dose of ETR NS loaded DMNs and ETR loaded DMNs patches in female rats (n = 5 & 4 per treatment group).

normalization [11]. The T_{max} for the suspension of the marketed tablet was 2 h, whereas here it was delayed to 168 h for ETR NS- and ETR-loaded DMNs DMNs formulation. After dose normalization, there were 29.07 and 26.09-fold increases in the AUC for ETR NS- and ETR powder-loaded DMNs compared to the commercial Intelence® 200 mg/kg tablet, suggesting clinical potential of our DMNs [28,85].

3.6. Conclusion

Here, we have, for the first time, developed a dissolving microneedle system capable of intradermal deposition of controlled release etravirine formulations. Using etravirine powder achieved similar pharmacokinetic performance to the nanosuspension, suggesting production could be simplified, reducing cost. Both microneedle formulations exhibited sustained delivery in rats *in vivo*, suggesting that, following further development, such patches may be clinically useful, in that they could replace daily tablets, thus potentially enhancing adherence to therapy and health-related quality of life for HIV patients.

Acknowledgements

This work was supported by EPSRC (EP/S028919/1) and The Wellcome Trust (WT094085MA). We also acknowledge support from the Department of Biotechnology, India, and the British Council, United Kingdom, under the Newton-Bhabha fund.

Appendix A. Supplementary material

Supplementary data to this article can be found online at https://doi.org/10.1016/j.ejpb.2021.04.024.

References

[1] L. Nabha, L. Duong, J. Timpone, HIV-associated neurocognitive disorders: Perspective on management strategies, Drugs 73 (2013) 893–905, https://doi.org/10.1007/s40265-013-0059-6.
[2] V.S. Saste, S.S. Kale, M.K. Sapate, D.T. Baviskar, Modern aspects for antiretroviral treatment, Int. J. Pharm. Sci. Rev. Res. 9 (2011) 18–24.
[3] J. Ananworanich, U. Siangphoe, A. Hill, P. Cardiello, W. Apateerapong, B. Hirschel, A. Mahanontharit, S. Ubolyam, D. Cooper, P. Phanuphak, K. Ruxrungtham, Highly active antiretroviral therapy (HAART) retreatment in patients on CD4-guided therapy achieved similar virologic suppression compared with patients on continuous HAART the HIV Netherlands Australia Thailand research collaboration 001.4 study, J. Acquir. Immune Defic. Syndr. 39 (2005) 523–529, https://doi.org/10.1097/01.qai.0000171636.81078.32.
[4] M.J. Gomes, J. das Neves, B. Sarmento, Nanoparticle-based drug delivery to improve the efficacy of antiretroviral therapy in the central nervous system, Int. J. Nanomed. 9 (2014) 1757–1769, https://doi.org/10.2147/IJN.S45886.
[5] P.E. Williams, H.M. Crauwels, E.D. Basstanie, Formulation and pharmacology of long-acting rilpivirine, Curr. Opin. HIV AIDS 10 (2015) 233–238, https://doi.org/10.1097/COH.0000000000000164.
[6] M. Lamorde, S. Walimbwa, P. Byakika-Kibwika, M. Katwere, L. Mukisa, J. B. Sempa, L. Else, D.J. Back, S.H. Khoo, C. Merry, Steady-state pharmacokinetics of rilpivirine under different meal conditions in HIV-1-infected Ugandan adults, J. Antimicrob. Chemother. 70 (2014) 1482–1486, https://doi.org/10.1093/jac/dku575.
[7] A.N. Nyaku, S.G. Kelly, B.O. Taiwo, Long-Acting Antiretrovirals: Where Are We now? Curr. HIV/AIDS Rep. 14 (2017) 63–71, https://doi.org/10.1007/s11904-017-0353-0.
[8] D.T. Jayaweera, L. Espinoza, J. Castro, Etravirine: The renaissance of non-nucleoside reverse transcriptase inhibitors, Expert Opin. Pharmacother. 9 (2008) 3083–3094, https://doi.org/10.1517/14656560802489569.
[9] L.B. Johnson, L.D. Saravolatz, Etravirine, a Next-Generation Nonnucleoside Reverse-Transcriptase Inhbitor, Clin. Infect. Dis. 48 (2009) 1123–1128, https://doi.org/10.1086/597469.
[10] T.N. Kakuda, G. De Smedt, R. Leemans, M. Peeters, V. Vyncke, R. Van Solingen-ristea, B. Woodfall, R. Hoetelmans, Bioavailability of etravirine 200mg administered as a single 200-mg tablet versus two 100-mg tablets in HIV-negative, healthy volunteers (2011) 20605.
[11] J. John, D. Liang, Oral liquid formulation of etravirine for enhanced bioavailability, J. Bioequivalence Bioavailab. 6 (2014) 46–52, https://doi.org/10.4172/jbb.1000179.
[12] M.R. Prausnitz, R. Langer, Transdermal drug delivery, Nat. Biotechnol. 26 (2008) 1261–1268, https://doi.org/10.1038/nbt.1504.
[13] A. Alkilani, M.T. McCrudden, R. Donnelly, Transdermal Drug Delivery: Innovative Pharmaceutical Developments Based on Disruption of the Barrier Properties of the Stratum Corneum, Pharmaceutics 7 (2015) 438–470, https://doi.org/10.3390/pharmaceutics7040438.
[14] A.J. Mohammad Zaki, S.K. Patil, D.T. Baviskar, D.K. Jain, Implantable drug delivery system: A review, Int. J. PharmTech Res. 4 (2012) 280–292.
[15] L.K. Vora, K. Moffatt, I.A. Tekko, A.J. Paredes, F. Volpe-Zanutto, D. Mishra, K. Peng, R. Raj Singh Thakur, R.F. Donnelly, Microneedle array systems for long-acting drug delivery, Eur. J. Pharm. Biopharm. 159 (2021) 44–76, https://doi.org/10.1016/j.ejpb.2020.12.006.
[16] L.K. Vora, P.R. Vavia, E. Larrañeta, S.E.J. Bell, R.F. Donnelly, Novel nanosuspension-based dissolving microneedle arrays for transdermal delivery of a hydrophobic drug, J. Interdiscip. Nanomed. 3 (2018) 89–101, https://doi.org/10.1002/jin2.41.
[17] S. Henry, D.V. McAllister, M.G. Allen, M.R. Prausnitz, Microfabricated microneedles: A novel approach to transdermal drug delivery, J. Pharm. Sci. 87 (1998) 922–925, https://doi.org/10.1021/js980042+.
[18] E.M. Vicente-Pérez, H.L. Quinn, E. McAlister, S. O'Neill, L.-A. Hanna, J.G. Barry, R. F. Donnelly, The Use of a Pressure-Indicating Sensor Film to Provide Feedback upon Hydrogel-Forming Microneedle Array Self-Application In Vivo, Pharm. Res. 33 (2016) 3072–3080, https://doi.org/10.1007/s11095-016-2032-z.
[19] M. Bagga, A. Ghosh, M. Deka, Microneedles in transdermal drug delivery, Indian Drugs. 47 (2010) 7–15.
[20] H.L. Quinn, M.C. Kearney, A.J. Courtenay, M.T. McCrudden, R.F. Donnelly, The role of microneedles for drug and vaccine delivery, Expert Opin. Drug Deliv. 11 (2014) 1769–1780, https://doi.org/10.1517/17425247.2014.938635.
[21] W.R. Spreen, D.A. Margolis, J.C. Pottage, Long-acting injectable antiretrovirals for HIV treatment and prevention, Curr. Opin. HIV AIDS 8 (2013) 565–571, https://doi.org/10.1097/COH.0000000000000002.
[22] Á. Cárcamo-Martínez, B. Mallon, Q.K. Anjani, J. Domínguez-Robles, E. Utomo, L. K. Vora, I.A. Tekko, E. Larrañeta, R.F. Donnelly, Enhancing intradermal delivery of tofacitinib citrate: Comparison between powder-loaded hollow microneedle arrays and dissolving microneedle arrays, Int. J. Pharm. 593 (2021), https://doi.org/10.1016/j.ijpharm.2020.120152.
[23] Q.K. Anjani, A.D. Permana, Á. Cárcamo-Martínez, J. Domínguez-Robles, I. A. Tekko, E. Larrañeta, L.K. Vora, D. Ramadon, R.F. Donnelly, Versatility of hydrogel-forming microneedles in in vitro transdermal delivery of tuberculosis drugs, Eur. J. Pharm. Biopharm. 158 (2021) 294–312, https://doi.org/10.1016/j.ejpb.2020.12.003.
[24] Q.K. Anjani, A.D. Permana, Á. Cárcamo-Martínez, J. Domínguez-Robles, I. A. Tekko, E. Larrañeta, L.K. Vora, D. Ramadon, R.F. Donnelly, Versatility of hydrogel-forming microneedles in in vitro transdermal delivery of tuberculosis drugs, Eur. J. Pharm. Biopharm. 158 (2021) 294–312, https://doi.org/10.1016/j.ejpb.2020.12.003.
[25] L.K. Vora, R.F. Donnelly, E. Larrañeta, P. González-Vázquez, R.R.S. Thakur, P. R. Vavia, Novel bilayer dissolving microneedle arrays with concentrated PLGA nano-microparticles for targeted intradermal delivery: Proof of concept, J. Control. Release (2017), https://doi.org/10.1016/j.jconrel.2017.10.005.
[26] M.Y. Kim, B. Jung, J.H. Park, Hydrogel swelling as a trigger to release biodegradable polymer microneedles in skin, Biomaterials 33 (2012) 668–678, https://doi.org/10.1016/j.biomaterials.2011.09.074.
[27] T. Waghule, G. Singhvi, S.K. Dubey, M.M. Pandey, G. Gupta, M. Singh, K. Dua, Microneedles: A smart approach and increasing potential for transdermal drug delivery system, Biomed. Pharmacother. 109 (2019) 1249–1258, https://doi.org/10.1016/j.biopha.2018.10.078.
[28] M.T.C. Mc Crudden, E. Larrañeta, A. Clark, C. Jarrahian, A. Rein-Weston, S. Lachau-Durand, N. Niemeijer, P. Williams, C. Haeck, H.O. McCarthy, D. Zehrung, R.F. Donnelly, Design, formulation and evaluation of novel dissolving microarray patches containing a long-acting rilpivirine nanosuspension, J. Control. Release 28 (2018) 119–129, https://doi.org/10.1016/j.jconrel.2018.11.002.
[29] A. Rein-Weston, I. Tekko, L. Vora, C. Jarrahian, B. Spreen, T. Scott, R. Donnelly, D. Zehrung, LB8. Microarray Patch Delivery of Long-Acting HIV PrEP and Contraception, Open Forum Infect. Dis. 6 (2019) S996, https://doi.org/10.1093/ofid/ofz415.2491.
[30] R.F. Donnelly, E. Larrañeta, Microarray patches: potentially useful delivery systems for long-acting nanosuspensions, Drug Discov. Today 23 (2018) 1026–1033, https://doi.org/10.1016/j.drudis.2017.10.013.
[31] E. Larrañeta, L. Vora, Delivery of Nanomedicines Using Microneedles, Microneedles Drug Vaccine Deliv, Patient Monit. (2018) 177–205, https://doi.org/10.1002/9781119305101.ch6.
[32] B. Sun, Y. Yeo, Nanocrystals for the parenteral delivery of poorly water-soluble drugs, Curr. Opin. Solid State Mater. Sci. 16 (2012) 295–301, https://doi.org/10.1016/j.cossms.2012.10.004.
[33] W.W.L. Chin, J. Parmentier, M. Widzinski, E.N.H. Tan, R. Gokhale, A brief literature and patent review of nanosuspensions to a final drug product, J. Pharm. Sci. 103 (2014) 2980–2999, https://doi.org/10.1002/jps.24098.
[34] A. Owen, S. Rannard, Strengths, weaknesses, opportunities and challenges for long acting injectable therapies: Insights for applications in HIV therapy, Adv. Drug Deliv. Rev. 103 (2016) 144–156, https://doi.org/10.1016/j.addr.2016.02.003.
[35] J. Kennedy, E. Larrañeta, M.T.C. McCrudden, C.M. McCrudden, A.J. Brady, S. J. Fallows, H.O. McCarthy, A. Kissenpfennig, R.F. Donnelly, In vivo studies investigating biodistribution of nanoparticle-encapsulated rhodamine B delivered via dissolving microneedles, J. Control. Release 265 (2017) 57–65, https://doi.org/10.1016/j.jconrel.2017.04.022.
[38] E. Larrañeta, R.E.M. Lutton, A.D. Woolfson, R.F. Donnelly, Microneedle arrays as transdermal and intradermal drug delivery systems: Materials science, manufacture and commercial development, Mater. Sci. Eng. R Rep. 104 (2016) 1–32, https://doi.org/10.1016/j.mser.2016.03.001.

[39] D. Xia, P. Quan, H. Piao, H. Piao, S. Sun, Y. Yin, F. Cui, Preparation of stable nitrendipine nanosuspensions using the precipitation–ultrasonication method for enhancement of dissolution and oral bioavailability, Eur. J. Pharm. Sci. 40 (2010) 325–334, https://doi.org/10.1016/j.ejps.2010.04.006.
[43] I.A. Tekko, A.D. Permana, L. Vora, T. Hatahet, H.O. McCarthy, R.F. Donnelly, Localised and sustained intradermal delivery of methotrexate using nanocrystal-loaded microneedle arrays: Potential for enhanced treatment of psoriasis, Eur. J. Pharm. Sci. 152 (2020), https://doi.org/10.1016/j.ejps.2020.105469.
[44] S. Taneja, S. Shilpi, K. Khatri, Formulation and optimization of efavirenz nanosuspensions using the precipitation-ultrasonication technique for solubility enhancement, Artif. Cells, Nanomed. Biotechnol. 44 (2016) 978–984, https://doi.org/10.3109/21691401.2015.1008505.
[45] V. Damjanovic, D. Thomas, The use of polyvinylpyrrolidone as a cryoprotectant in the freezing of human lymphocytes, Cryobiology 11 (1974) 312–316, https://doi.org/10.1016/0011-2240(74)90007-8.
[46] R.F. Donnelly, M.T.C. McCrudden, A.Z. Alkilani, E. Larrañeta, E. McAlister, A. J. Courtenay, M.C. Kearney, T.R. Raj Singh, H.O. McCarthy, V.L. Kett, E. Caffarel-Salvador, S. Al-Zahrani, A.D. Woolfson, Hydrogel-forming microneedles prepared from "super swelling" polymers combined with lyophilised wafers for transdermal drug delivery, PLoS One 9 (2014), https://doi.org/10.1371/journal.pone.0111547.
[47] V.D. Sundar, P. Divya, P. Sridevi, K. Akhila, M.D. Dhanaraju, Design, formulation and evaluation of nanosuspension for drug delivery of celecoxib, Int. J. Pharm. Res. 11 (2019) 139–146, https://doi.org/10.31838/ijpr/2019.11.01.013.
[48] S. Ghosh, A. Sailaja, B. Ravikumar, Analytical method development and validation of etravirine in its bulk dosage form by using reverse phase high performance liquid chromatography method as per international conference on harmonisation guidelines, Asian J. Pharm. Clin. Res. 8 (2015) 147–150.
[49] C. Runja, R.K. Pigili, P. Rk, Development and Validation of a New RP-HPLC Method for Estimation of Etravirine in Bulk and Pharmaceutical Dosage Form, Int. J. Pharma Sci. 3 (2013) 291–294.
[50] I. Conference, O.N. Harmonisation, O.F. Technical, R. For, R. Of, P. For, A. Of, Ich_ 2005, 1994 (2005).
[51] C.V. Abobo, L. Wu, J. John, M.K. Joseph, T.R. Bates, D. Liang, LC-MS/MS determination of etravirine in rat plasma and its application in pharmacokinetic studies, J. Chromatogr. B Anal. Technol. Biomed. Life Sci. 878 (2010) 3181–3186, https://doi.org/10.1016/j.jchromb.2010.09.016.
[52] A.S. Cordeiro, I.A. Tekko, M.H. Jomaa, L. Vora, E. McAlister, F. Volpe-Zanutto, M. Nethery, P.T. Baine, N. Mitchell, D.W. McNeill, R.F. Donnelly, Two-Photon Polymerisation 3D Printing of Microneedle Array Templates with Versatile Designs: Application in the Development of Polymeric Drug Delivery Systems, Pharm. Res. 37 (2020) 1–15, https://doi.org/10.1007/s11095-020-02887-9.
[53] A.M. Rodgers, M.T.C. McCrudden, E.M. Vincente-Perez, A.V. Dubois, R.J. Ingram, E. Larrañeta, A. Kissenpfennig, R.F. Donnelly, Design and characterisation of a dissolving microneedle patch for intradermal vaccination with heat-inactivated bacteria: A proof of concept study, Int. J. Pharm. 549 (2018) 87–95, https://doi.org/10.1016/j.ijpharm.2018.07.049.
[54] H.L. Quinn, L. Bonham, C.M. Hughes, R.F. Donnelly, Design of a Dissolving Microneedle Platform for Transdermal Delivery of a Fixed-Dose Combination of Cardiovascular Drugs, J. Pharm. Sci. 104 (2015) 3490–3500, https://doi.org/10.1002/jps.24563.
[55] B. Pamornpathomkul, T. Ngawhirunpat, I.A. Tekko, L. Vora, H.O. McCarthy, R. F. Donnelly, Dissolving polymeric microneedle arrays for enhanced site-specific acyclovir delivery, Eur. J. Pharm. Sci. 121 (2018) 200–209, https://doi.org/10.1016/j.ejps.2018.05.009.
[56] E. Larrañeta, J. Moore, E.M. Vicente-Pérez, P. González-Vázquez, R. Lutton, A. D. Woolfson, R.F. Donnelly, A proposed model membrane and test method for microneedle insertion studies, Int. J. Pharm. (2014), https://doi.org/10.1016/j.ijpharm.2014.05.042.
[57] I.A. Tekko, G. Chen, J. Domínguez-Robles, R.R.S. Thakur, I.M.N. Hamdan, L. Vora, E. Larrañeta, J.C. McElnay, H.O. McCarthy, M. Rooney, R.F. Donnelly, Development and characterisation of novel poly (vinyl alcohol)/poly (vinyl pyrrolidone)-based hydrogel-forming microneedle arrays for enhanced and sustained transdermal delivery of methotrexate, Int. J. Pharm. 586 (2020), 119580, https://doi.org/10.1016/j.ijpharm.2020.119580.
[58] S. Abdelghany, I.A. Tekko, L. Vora, E. Larrañeta, A.D. Permana, R.F. Donnelly, Nanosuspension-based dissolving microneedle arrays for intradermal delivery of curcumin, Pharmaceutics 11 (2019) 308, https://doi.org/10.3390/pharmaceutics11070308.
[59] ICH, (VICH, 2016) Guidance for Industry Bioequivalence: Blood Level Bioequivalence Study, 52 (2016).
[60] R.S. Dhumal, S.V. Biradar, S. Yamamura, A.R. Paradkar, P. York, Preparation of amorphous cefuroxime axetil nanoparticles by sonoprecipitation for enhancement of bioavailability, Eur. J. Pharm. Biopharm. 70 (2008) 109–115, https://doi.org/10.1016/J.EJPB.2008.04.001.
[61] B. Sinha, R.H. Müller, J.P. Möschwitzer, Bottom-up approaches for preparing drug nanocrystals: Formulations and factors affecting particle size, Int. J. Pharm. 453 (2013) 126–141, https://doi.org/10.1016/j.ijpharm.2013.01.019.
[62] A. Mehrotra, J.K. Pandit, Critical process parameters evaluation of modified nanoprecipitation method on lomustine nanoparticles and cytostatic activity study on L132 human cancer cell line, J. Nanomed. Nanotechnol. 3 (2012) 6, https://doi.org/10.4172/2157-7439.1000149.
[63] S. Gera, S. Talluri, N. Rangaraj, S. Sampathi, Formulation and Evaluation of Naringenin Nanosuspensions for Bioavailability Enhancement, AAPS PharmSciTech. 18 (2017) 3151–3162, https://doi.org/10.1208/s12249-017-0790-5.
[64] A. Ahmadi Tehrani, M.M. Omranpoor, A. Vatanara, M. Seyedabadi, V. Ramezani, Formation of nanosuspensions in bottom-up approach: theories and optimization, DARU J. Pharm. Sci. 27 (2019) 451–473, https://doi.org/10.1007/s40199-018-00235-2.
[65] C. Detroja, S. Chavhan, K. Sawant, Enhanced antihypertensive activity of candesartan cilexetil nanosuspension: formulation, characterization and pharmacodynamic study, Sci. Pharm. 79 (2011) 635–651, https://doi.org/10.3797/scipharm.1103-17.
[66] S. Verma, R. Gokhale, D.J. Burgess, A comparative study of top-down and bottom-up approaches for the preparation of micro/nanosuspensions, Int. J. Pharm. 380 (2009) 216–222, https://doi.org/10.1016/j.ijpharm.2009.07.005.
[67] K. Yamaguchi, T. Matsumoto, K. Kuwata, Proper calibration of ultrasonic power enabled the quantitative analysis of the ultrasonication-induced amyloid formation process, Protein Sci. 21 (2012) 38–49, https://doi.org/10.1002/pro.755.
[68] T. Ojha, V. Pathak, N. Drude, M. Weiler, D. Rommel, S. Rütten, B. Geinitz, M.J. Van Steenbergen, G. Storm, F. Kiessling, T. Lammers, Shelf-life evaluation and lyophilization of PBCA-based polymeric microbubbles, Pharmaceutics 11 (2019), https://doi.org/10.3390/pharmaceutics11090433.
[69] N.-O. Chung, M.K. Lee, J. Lee, Mechanism of freeze-drying drug nanosuspensions, Int. J. Pharm. 437 (2012) 42–50, https://doi.org/10.1016/j.ijpharm.2012.07.068.
[70] L. Vora, V.G. Sita, P. Vavia, Zero order controlled release delivery of cholecalciferol from injectable biodegradable microsphere: in-vitro characterization and in-vivo pharmacokinetic studies, Eur. J. Pharm. Sci. 107 (2017) 78–86, https://doi.org/10.1016/j.ejps.2017.06.027.
[71] L. Rajput, P. Sanphui, G.R. Desiraju, New solid forms of the anti-HIV drug etravirine: Salts, cocrystals, and solubility, Cryst. Growth Des. 13 (2013) 3681–3690, https://doi.org/10.1021/cg4007058.
[72] P. Kommavarapu, A. Maruthapillai, K. Palanisamy, R.T. Koya, Physical characterization and dissolution performance assessment of Etravirine solid dispersions prepared by spray drying process, Pak. J. Pharm. Sci. 29 (2016) 2023–2031.
[73] I. Weuts, F. Van Dycke, J. Voorspoels, S. De Cort, S. Stokbroekx, R. Leemans, M. E. Brewster, D. Xu, B. Segmuller, Y.T.A. Turner, C.J. Roberts, M.C. Davies, S. Qi, D. Q.M. Craig, M. Reading, Physicochemical Properties of the Amorphous Drug, Cast Films, and Spray Dried Powders to Predict Formulation Probability of Success for Solid Dispersions: Etravirine, J. Pharm. Sci. 100 (2011) 260–274, https://doi.org/10.1002/jps.22242.
[74] H. Thakkar, S. Thakkar, B. Patel, Development and characterization of nanosuspensions of olmesartan medoxomil for bioavailability enhancement, J. Pharm. Bioallied Sci. 3 (2011) 426, https://doi.org/10.4103/0975-7406.84459.
[75] V.B. Patravale, A.A. Date, R.M. Kulkarni, Nanosuspensions: a promising drug delivery strategy, J. Pharm. Pharmacol. 56 (2004) 827–840, https://doi.org/10.1211/0022357023691.
[76] M.T.C. McCrudden, A.Z. Alkilani, C.M. McCrudden, E. McAlister, H.O. McCarthy, A.D. Woolfson, R.F. Donnelly, Design and physicochemical characterisation of novel dissolving polymeric microneedle arrays for transdermal delivery of high dose, low molecular weight drugs, J. Control. Release 180 (2014) 71–80, https://doi.org/10.1016/J.JCONREL.2014.02.007.
[77] M. Garg, A. Asthana, H.B. Agashe, G.P. Agrawal, N.K. Jain, Stavudine-loaded mannosylated liposomes: in-vitro anti-HIV-I activity, tissue distribution and pharmacokinetics, J. Pharm. Pharmacol. 58 (2006) 605–616, https://doi.org/10.1211/jpp.58.5.0005.
[78] A. Bhakay, M. Rahman, R.N. Dave, E. Bilgili, Bioavailability enhancement of poorly water-soluble drugs via nanocomposites: Formulation-Processing aspects and challenges, Pharmaceutics 10 (2018), https://doi.org/10.3390/pharmaceutics10030086.
[79] A. Raju, A. Reddy, J. Satheesh, A. V. Jithan, Preparation and characterisation of nevirapine oral nanosuspensions 1. Raju A, Reddy A, Satheesh J, Jithan A V. Preparation and characterisation of nevirapine oral nanosuspensions. Indian J Pharm Sci. 2014;76(1):62-71. /pmc/articles/PMC4007257/?report=abst, Indian J. Pharm. Sci. 76 (2014) 62–71.
[80] M.R. Bhalekar, P.G. Upadhaya, A.R. Madgulkar, S.J. Kshirsagar, A. Dube, U. S. Bartakke, In-vivo bioavailability and lymphatic uptake evaluation of lipid nanoparticulates of darunavir, Drug Deliv. 23 (2016) 2581–2586, https://doi.org/10.3109/10717544.2015.1037969.
[81] R. Shegokar, K.K. Singh, Surface modified nevirapine nanosuspensions for viral reservoir targeting: In vitro and in vivo evaluation, Int. J. Pharm. 421 (2011) 341–352, https://doi.org/10.1016/j.ijpharm.2011.09.041.
[82] S. Singh, S. Purvin, P.R. Vuddanda, S.K. Singh, A. Jain, Pharmacokinetic and tissue distribution study of solid lipid nanoparticles of zidovudine in rats, J. Nanotechnol. 2014 (2014), https://doi.org/10.1155/2014/854018.
[83] T. Chakraborty, M.K. Das, L. Dutta, B. Mukherjee, S. Das, A. Sarma, Successful Delivery of Zidovudine-Loaded Docosanol Nanostructured Lipid Carriers (Docosanol NLCs) into Rat Brain, in: Surf. Modif. Nanoparticles Target. Drug Deliv., Springer International Publishing, 2019, pp. 245–276, https://doi.org/10.1007/978-3-030-06115-9_14.
[84] E. Seminari, A. Castagna, A. Lazzarin, Etravirine for the treatment of HIV infection, Expert Rev. Anti. Infect. Ther. 6 (2008) 427–433, https://doi.org/10.1586/14787210.6.4.427.
[85] G. Van 't Klooster, E. Hoeben, H. Borghys, A. Looszova, M.P. Bouche, F. Van Velsen, L. Baert, Pharmacokinetics and disposition of rilpivirine (TMC278) nanosuspension as a long-acting injectable antiretroviral formulation, Antimicrob. Agents Chemother. 54 (2010) 2042–2050, https://doi.org/10.1128/AAC.01529-09.